

Beyond asymptotic reasoning: a practical ground state projector based on the wall-Chebyshev expansion

Maria-Andreea Filip*

Yusuf Hamied Department of Chemistry, University of Cambridge,
Lensfield Road, Cambridge CB2 1EW, United Kingdom

Nathan Fitzpatrick†

Quantinuum, 13-15 Hills Road, CB2 1NL, Cambridge, United Kingdom

We introduce a quantum algorithm for ground-state preparation based on a Chebyshev series approximation to the wall function. This projector can be efficiently implemented as a product of Hamiltonian operators, enabling a straightforward realization via the linear combinations of unitaries method. We analyze the asymptotic scaling and provide numerical benchmarks, demonstrating that the wall-Chebyshev projector achieves competitive performance with leading methods based on imaginary time evolution and alternative projector function approximations. Notably, our approach exhibits superior robustness and convergence in scenarios where accurate ground-state energy estimates are unavailable, showing promise for realistic chemistry problems.

I. INTRODUCTION

Imaginary time evolution (ITE) is an effective means to obtain the ground state of quantum systems. The formalism is obtained by a Wick rotation[1] of the time-dependent Schrödinger equation

$$i \frac{\partial \Psi(t)}{\partial t} = \hat{H} \Psi(t), \quad (1)$$

by transforming $it \rightarrow \tau$ to give the so-called imaginary time Schrödinger equation

$$\frac{\partial \Psi(\tau)}{\partial \tau} = -\hat{H} \Psi(\tau), \quad (2)$$

where \hat{H} is the problem Hamiltonian, Ψ is the system wavefunction and τ is imaginary time. Eq. (2) has a solution of the form

$$\Psi(\tau) = C e^{-\hat{H}\tau} \Psi(0), \quad (3)$$

where C is some constant of integration. Given a set $\{\Psi_i\}$ of eigenfunctions of the Hamiltonian, with corresponding eigenvalues $\{E_i\}$, the wavefunction may be decomposed into

$$\Psi(\tau) = C \sum_i c_i e^{-E_i \tau} \Psi_i, \quad (4)$$

where $\Psi(0) = \sum_i c_i \Psi_i$. Therefore, as $\tau \rightarrow \infty$, the right-hand-side of Eq. (4) will be dominated by the wavefunction with the lowest E_i , so

$$\lim_{\tau \rightarrow \infty} \Psi(\tau) \propto \Psi_0. \quad (5)$$

Imaginary time evolution therefore provides a valuable alternative to variational wavefunction optimization. In

the full Hilbert space, there is only one minimum of energy[2], but using restricted wavefunction ansätze leads to the appearance of local minima, generating very complex energy landscapes[3]. This can cause conventional optimization algorithms to become stuck, while imaginary time evolution is guaranteed to converge to the global minimum of the ansatz, provided a sufficiently long time interval. Additionally, in the context of quantum computing, it allows for ansatz-free wavefunction optimization, allowing the overall Hilbert space ground state to be found. However, unlike the real time propagator $e^{-i\hat{H}t}$, the imaginary time propagator $e^{-\hat{H}\tau}$ is nonunitary, making it challenging to implement on a quantum computer. Various approaches have been developed to address this problem.

Variational imaginary time evolution[4–6] (VITE) uses an ansatz to approximate the imaginary time-evolved wavefunction and then optimizes it according to some variational principle[7]. This is a hybrid quantum-classical algorithm and therefore appropriate for noisy intermediate-scale quantum (NISQ) devices. However, the original implementation of VITE[4, 5] requires matrix inversions to obtain the ansatz parameters and is therefore highly susceptible to noise. Additionally, like most variational quantum algorithms, VITE may suffer from optimization problems, such as barren plateaus[8], which preclude convergence.

In quantum imaginary time evolution (QITE)[9–11], the renormalized action of the imaginary time propagator is mapped onto a unitary operator, which can be determined from multiple sets of linear equations. The storage and measurement required scales as the exponential of the correlation length, which increases during the course of the time evolution. This scaling can be improved by imposing additional locality constraints[9]. Alternatively, circuit depth can be reduced by lifting the locality constraint[10].

Finally, probabilistic imaginary time evolution (PITE)[12–16] uses a block-encoded form of the imag-

* maf63@cam.ac.uk

† nathan.fitzpatrick@quantinuum.com

inary time evolution operator. This is often done by encoding a short-time propagation operator and applying it repeatedly. While this decreases the error in the encoding of the operator itself, the probability of success decays exponentially with the number of repetitions. In addition to reasonably deep circuits and ancilla qubit requirements, which scale logarithmically with the number of terms in the Hamiltonian for linear combination of unitaries (LCU) based encoding approaches, this makes PITE methods more suitable for fault-tolerant quantum computers than current NISQ devices.

Encodings which do away with the need for repeated application of the unitary as well as the large number of ancillas have also been developed. One such approach uses the Quantum Eigenvalue Transform with Unitary block-encoding[17] (QETU) of a polynomial approximation to the imaginary time evolution operator[18].

Alternative polynomial expansions can also be used to project onto the ground state of a quantum system of interest. In conventional quantum chemistry, particularly in the area of Monte Carlo simulations[19–22], it is common to employ the first-orderer Taylor expansion of the imaginary time-evolution operator,

$$e^{-\hat{H}\delta\tau} \approx 1 - \delta\tau\hat{H}, \quad (6)$$

as a projector, with the ground state obtained in the infinite-time limit as

$$\Psi_0 = \lim_{n \rightarrow \infty} (1 - \delta\tau\hat{H})^n \Psi(0). \quad (7)$$

In a quantum setting, the hybrid Projective Quantum Eigensolver (PQE) method is based on this projection approach[23].

The original QETU[17] approach employed a polynomial approximation of a shifted step function

$$\text{step}(x) = \begin{cases} 1, & x \leq \mu \\ 0, & x > \mu \end{cases} \quad (8)$$

for ground state preparation. In the absence of a good estimate of the ground state energy, this may be employed as a projector onto a low-energy subspace, which can be combined with binary search approaches to find the ground state[24]. A more general approach for arbitrary eigenvalue filtering uses a quantum signal processing (QSP) implementation of

$$R_l(x; \Delta) = \frac{T_l(-1 + 2\frac{x^2 - \Delta^2}{1 - \Delta^2})}{T_l(-1 + 2\frac{-\Delta^2}{1 - \Delta^2})}, \quad (9)$$

where $T_l(x)$ is the l -th Chebyshev polynomial of the first kind, defined as

$$T_l(\cos \theta) = \cos(l\theta), \quad (10)$$

and Δ is the spectral gap of the intended eigenvalue[25]. Chebyshev polynomials have also been used in conventional quantum chemistry to implement a projector based

on the wall function[26, 27],

$$\text{wall}(x) = \begin{cases} \infty, & x \leq -1 \\ 1, & x = -1 \\ 0, & x > -1. \end{cases} \quad (11)$$

This can be considered as the limit as τ tends to infinity of the exponential propagator

$$\lim_{\tau \rightarrow \infty} e^{-\tau(x-S)} = \text{wall}(x - S), \quad (12)$$

and we can see that it must recover the ground state wavefunction.

In this work, we introduce a quantum algorithm for ground state preparation based on the wall-Chebyshev projector, and benchmark its practical performance against leading approaches such as quantum imaginary time evolution, step functions and eigenvalue filtering. We demonstrate that this method achieves superior asymptotic query complexity and better numerical performance, particularly in scenarios where accurate ground-state energy estimates are unavailable. It is shown that in these regimes step function and eigenstate filtering projector techniques often fail. Furthermore, the wall-Chebyshev projector naturally supports an iterative application, enabling systematic refinement of the ground-state estimate and robust convergence even in challenging cases such as the strongly correlated Hubbard model. The query complexity for single projector application is shown in Table I.

Method	Scaling
wall-Chebyshev	$\mathcal{O}(\Delta^{-1/2} (\log(\epsilon^{-1} c_0^{-1}))^{1/2})$
Imaginary time evolution[15]	$\mathcal{O}(\Delta^{-1} \log(\epsilon^{-1} c_0^{-1}))$
Eigenstate filter[25]	$\mathcal{O}(\Delta^{-1} \log(\epsilon^{-1} c_0^{-1}))$
Step function[24]	$\mathcal{O}(\Delta^{-1} \log(\epsilon^{-1} c_0^{-1}))$

TABLE I. Asymptotic scaling of the query complexity with respect to error for the wall-Chebyshev projector described in this work and alternative ground-state projection algorithms. Here, Δ is the gap between the ground and first excited states of the Hamiltonian, c_0 is the initial overlap with the ground state and ϵ is the target error. For comparison, we list the asymptotic scaling of comparable projection algorithms. Brief derivations of these scalings, following Refs. [15, 24, 25], are given in Appendix E.

II. THE WALL-CHEBYSHEV PROJECTOR

Chebyshev polynomials are naturally defined on the interval $[-1, 1]$. An m -th order Chebyshev expansion of

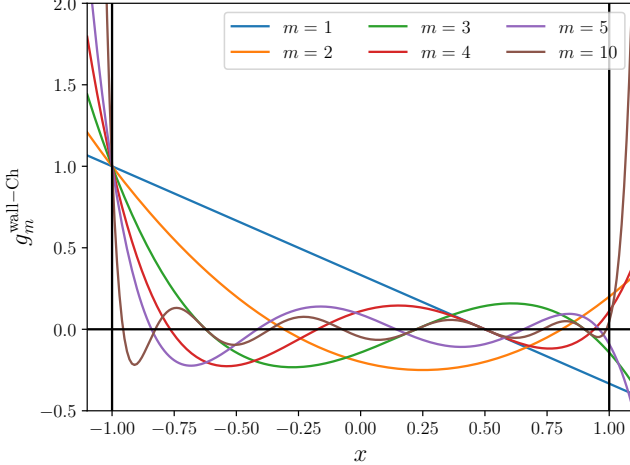


FIG. 1. Different order Chebyshev polynomial expansions of the wall function.

the wall function (Eq. (11)) on this interval is given by

$$\begin{aligned} G_m^{\text{wall-Ch}}(x) &= \frac{1}{1+2m} \sum_{k=0}^m (2 - \delta_{k0})(-1)^k T_k(x) \\ &= \frac{1}{1+2m} \sum_{k=0}^m (2 - \delta_{k0}) T_k(-x), \end{aligned} \quad (13)$$

where, δ_{ij} is the Kronecker delta. Some examples are shown in Fig. 1. We can map the Hamiltonian eigenspectrum onto the $[-1, 1]$ interval through the transformation

$$x = 2 \frac{\hat{H} - E_0}{R} - 1, \quad (14)$$

where $R = E_{\max} - E_0$ is the spectral range of the Hamiltonian, giving

$$g_m^{\text{wall-Ch}}(\hat{H}) = \frac{1}{1+2m} \sum_{k=0}^m (2 - \delta_{k0}) T_k \left(1 - 2 \frac{\hat{H} - E_0}{R} \right). \quad (15)$$

This polynomial decomposition has a series of nodes in the interval $[E_0, E_0 + R]$ at

$$a_\nu = E_0 + \frac{R}{2} \left(1 - \cos \frac{\nu\pi}{m+1/2} \right). \quad (16)$$

See, for example, Appendix B in Ref. [27] for a proof. We can then write:

$$g_m^{\text{wall-Ch}}(\hat{H}) = \prod_{\nu=1}^m \frac{\hat{H} - a_\nu}{E_0 - a_\nu}. \quad (17)$$

As this is not an exact representation of the wall function, further increased overlap with the ground state may be obtained by repeating the application of this projector. We define

$$|\Psi^{(n,0)}\rangle = [g^{\text{wall-Ch}}(\hat{H})]^n |\Phi\rangle \quad (18)$$

as the wavefunction after an integer number of applications of the projector and additionally define intermediate wavefunctions as

$$|\Psi^{(n,\mu)}\rangle = \left[\prod_{\nu=0}^{\mu} \frac{\hat{H} - a_\nu}{S - a_\nu} \right] [g^{\text{wall-Ch}}(\hat{H})]^n |\Phi\rangle. \quad (19)$$

where S is an estimate of the unknown E_0 .

In principle, for a given number N of applications of the Hamiltonian, applying the order- N wall-Chebyshev projector will give a better ground-state approximation than applying a lower order- m projector N/m times. However, lower-order projectors are generally more numerically stable, which may lead to better overall performance[27]. Additionally, in a classical setting, repeated projection allows recomputation of S between the application of different projectors, which can be used to assess convergence and increase the accuracy of the projector.

Implementing this projector requires estimates for the ground and highest excited states of the Hamiltonian. The latter can be estimated using an approximation to the Gershgorin circle theorem[28] (see Appendix A) as

$$\tilde{E}_{N-1} = H_{N-1,N-1} + \sum_{j \neq N-1} |H_{N-1,j}|. \quad (20)$$

Using the same estimator for the ground state energy S , we define the estimated spectral range of the Hamiltonian as

$$R = \alpha \tilde{E}_{N-1} - S \quad (21)$$

with $\alpha \geq 1$ to ensure the true spectral range of the Hamiltonian is less than R . This is important as, unlike the exact wall function, the Chebyshev approximation diverges not only for $x < -1$, but also for $x > 1$. The ground-state energy estimator may be initialised to the energy of the reference wavefunction $|\Phi\rangle$ and, if repeated applications of the projector are needed, it can be updated over the course of the propagation using the intermediate wavefunction $|\Psi^{(n,0)}\rangle$. For this purpose, one would need to estimate the expectation value of the energy $\langle \Psi^{(n,0)} | \hat{H} | \Psi^{(n,0)} \rangle$, which would require repetitions of the projection circuit. In practice, we find that, provided the original estimate of the ground state energy is higher than the true value, recomputing it is generally unnecessary.

III. QUANTUM IMPLEMENTATION

For an s -qubit operator A , a unitary matrix U acting on $s+b$ qubits corresponds to a (α, b, ε) -block encoding of A if

$$\|A - \alpha(\langle \Pi |^b \otimes I)U(|\Pi\rangle^b \otimes I)\| \leq \varepsilon \quad (22)$$

For $\varepsilon = 0$, this corresponds to

$$A = \alpha(\langle \Pi |^b \otimes I)U(|\Pi\rangle^b \otimes I) \quad (23)$$

and U has the form

$$U = \begin{pmatrix} |\Pi\rangle\langle\psi| & |\Pi_\perp\rangle\langle\psi| \\ A/\alpha & * \\ * & * \end{pmatrix} \langle\Pi|\langle\psi| \langle\Pi_\perp|\langle\psi|. \quad (24)$$

$|\Pi\rangle$ is typically the $|0\rangle^{\otimes b}$ state and $|\psi\rangle$ is the wavefunction of the system register. The sub-normalisation α must be such that $\|A\|/\alpha \leq 1$, where $\|\cdot\|$ denotes the spectral norm of an operator. The success probability of applying a block-encoded operator is then given by

$$P = \frac{\langle\psi|\hat{A}^\dagger A|\psi\rangle}{a^2}. \quad (25)$$

A variety of options are available to obtain block-encodings of operators. Here we use the linear combination of unitaries (LCU) approach [29], detailed in appendix B, to encode the Hamiltonian. A popular approach for block encoding polynomial functions of operators, is Quantum Singular Values Transformation (QSVT),[30] some details of which are given Appendix C. However, this approach is limited to polynomial functions P which obey the following constraints:

- (i) P has parity $d \bmod 2$
- (ii) $\forall x \in [-1, 1] : |P(x)| \leq 1$
- (iii) $\forall x \in (-\infty, -1] \cup [1, \infty) : |P(x)| \geq 1$
- (iv) if d is even, then $\forall x \in \mathbb{R} : P(ix)P^*(ix) \geq 1$.

The wall-Chebyshev projector obeys constraints (ii) and (iii) above. However, it does not have a well-defined parity on the $[-1, 1]$ interval, as can be clearly seen when considering the linear terms in Eq. (17). Therefore, it is not amenable to implementation by standard QSVT. The odd and even parts of the polynomial could be encoded separately, as is customarily done for the (imaginary) time-evolution operator[15, 31, 32], or the projector could be encoded by generalised Quantum Signal Processing (QSP)[33]. Alternatively, one may obtain encodings of the non-unitary operators $\hat{H}_\nu = \frac{\hat{H}-a_\nu}{S-a_\nu}$ and apply them sequentially, which is the approach followed in this work.

We note that, for the operators \hat{H}_ν , the denominator will be absorbed in the sub-normalisation. Given an $(\alpha, b, 0)$ encoding of the Hamiltonian, it is easy to obtain an $(\alpha + |a_\nu|, b + 1, 0)$ encoding for each of these operators[30]. However, since in most realistic scenarios the Hamiltonian \hat{H} will include a diagonal term and the values a_ν are known *a priori* for a given value of S , it is more efficient to generate ν different $(\alpha, b, 0)$ oracles corresponding to each term in the expansion.

The wall-Chebyshev projector can then be implemented as a series of rescaled block-encoding unitaries $U\left(\frac{\hat{H}-a_\nu}{S-a_\nu}\right)$. The projection is achieved by successive applications of $U\left(\frac{\hat{H}-a_1}{S-a_1}\right), \dots, U\left(\frac{\hat{H}-a_m}{S-a_m}\right)$, with the projection applied after each U via mid-circuit measurement on the $|0 \dots 0\rangle$ state, as shown in Fig. 2.

IV. COMPLEXITY ANALYSIS

The fidelity of the wavefunction obtained after applying a wall-Chebyshev projector of order m , labelled g in the following, is given by

$$\begin{aligned} f &= \frac{\langle\Psi_0|\Psi\rangle}{\sqrt{\langle\Psi^{(n)}|\Psi^{(n)}\rangle}} = \frac{c_0 g(E_0)}{\sqrt{\sum_i |c_i|^2 |g(E_i)|^2}} \\ &= \frac{1}{\sqrt{1 + \sum_{i>0} \left| \frac{c_i}{c_0} \right|^2 \left| \frac{g(E_i)}{g(E_0)} \right|^2}} \\ &\geq \frac{1}{1 + \sqrt{\sum_{i>0} \left| \frac{c_i}{c_0} \right|^2 \left| \frac{g(E_i)}{g(E_0)} \right|^2}} \\ &\geq \frac{1}{1 + \frac{1}{|c_0|} \max_{i>0} \left(\left| \frac{g(E_i)}{g(E_0)} \right| \right) \sqrt{\sum_{i>0} |c_i|^2}} \\ &= \frac{1}{1 + \frac{1}{|c_0|} \max_{i>0} \left(\left| \frac{g(E_i)}{g(E_0)} \right| \right) \sqrt{1 - |c_0|^2}} \\ &\geq \frac{1}{1 + \frac{1}{|c_0|} \max_{i>0} \left(\left| \frac{g(E_i)}{g(E_0)} \right| \right)}. \end{aligned} \quad (26)$$

We can assume without loss of generality that c_0 is real and positive. In the limit of large m , g decays with E , so $\max_{i>0} \left(\left| \frac{g(E_i)}{g(E_0)} \right| \right) = \left| \frac{g(E_1)}{g(E_0)} \right|$. Therefore,

$$f \geq \frac{1}{1 + \frac{1}{c_0} \left| \frac{g(E_1)}{g(E_0)} \right|}. \quad (27)$$

$\left| \frac{g(E_i)}{g(E_0)} \right|$ can be approximated as

$$\left| \frac{g(E_i)}{g(E_0)} \right| \approx |1 + (E_1 - E_0)g'(E_0)| \equiv |1 - \Delta\gamma| \approx \exp(-\Delta\gamma), \quad (28)$$

where $\gamma = -g'(E_0)$ is called the convergence factor of g [26]. For the wall-Chebyshev projector, we derive γ in Appendix D and find it to be

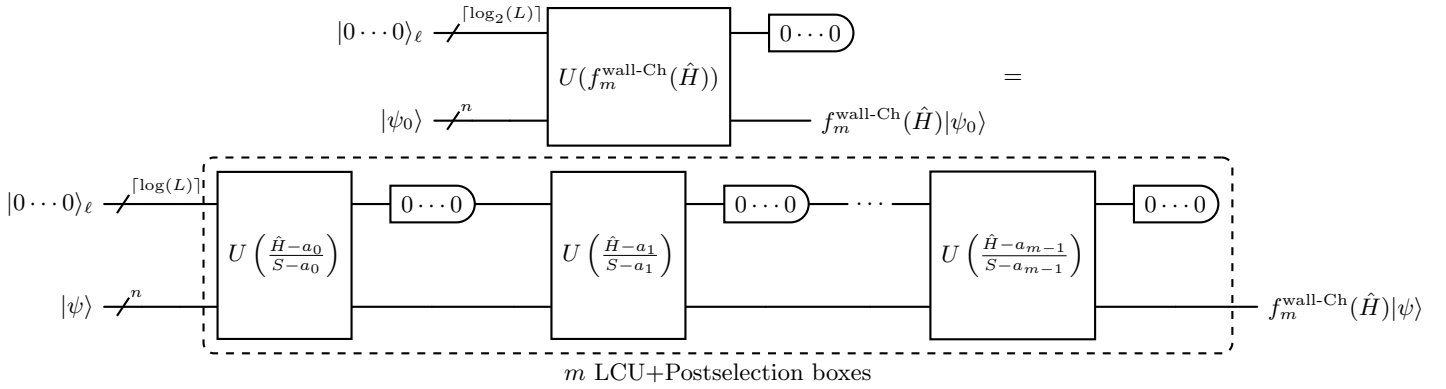
$$\gamma = \frac{2m(m+1)}{3R}. \quad (29)$$

Therefore

$$\begin{aligned} \epsilon = 1 - f &\leq 1 - \frac{1}{1 + \frac{\exp(-\Delta\gamma)}{c_0}} \\ &\leq \frac{\exp\left(-\frac{2\Delta m(m+1)}{3R}\right)}{c_0} \end{aligned} \quad (30)$$

and the required polynomial order for a given error ϵ scales as

$$m = \mathcal{O}\left(\Delta^{-1/2}(\log(\epsilon^{-1}c_0^{-1}))^{1/2}\right), \quad (31)$$

FIG. 2. LCU circuit for the wall-Chebyshev projector of order m .

which represents a polynomial improvement in asymptotic scaling relative to comparable projectors detailed in Appendix E.

While the scaling of m with system size is very favourable, we note that the alternative approach of applying a fixed-order projector repeatedly also scales competitively. The error in the fidelity after applying the projector g n times is given by

$$\epsilon^{(n)} \leq \frac{1}{1 + \frac{1}{c_0} \left| \frac{g(E_1)}{g(E_0)} \right|^n}, \quad (32)$$

so the number of applications of the Hamiltonian scales as

$$n = \mathcal{O}(\Delta^{-1} \log(\epsilon^{-1} c_0^{-1})), \quad (33)$$

which is on par with state-of-the-art projectors.

V. NUMERICAL COMPARISONS

To assess the practical performance of the wall-Chebyshev projector, we compare it to the step function projector in Ref. [24], the eigenstate filtering approach in Ref. [25] and an imaginary time evolution projector based on the Chebyshev expansion in Ref. [15]. Circuit implementations and simulations of the wall-Chebyshev projector incorporating mid-circuit measurements were performed using the `wallcheb` package [34], within the `Guppy` quantum circuit framework [35]. The resulting circuits were compiled via the multiplexor LCU block-encoding method as described in Ref. [36]. The coefficients for the step function projector were obtained using `QSPPACK`[37–40]. For the imaginary time evolution, there are two free parameters, the polynomial order *per* time-step and the size of the imaginary time-step. To reduce this to one parameter, we use the first-order approximation,

$$e^{-\tau H} \approx I_0(\tau) - 2I_1(\tau)T_1(H), \quad (34)$$

where I_l are modified Bessel functions of the first kind. We set the time-step such that the truncation error of this approximation is less than 0.01.

As a first test case, we consider the Hubbard model, with Hamiltonian

$$\hat{H} = -t \sum_{i,\sigma} (c_{i,\sigma}^\dagger c_{i+1,\sigma} + c_{i+1,\sigma}^\dagger c_{i,\sigma}) + U \sum_i n_{i\uparrow} n_{i\downarrow}, \quad (35)$$

where $c_{i,\sigma}^\dagger$ and $c_{i,\sigma}$ are creation and annihilation operators for electrons with $m_s = \sigma$ at site i , respectively, and $n_{i,\sigma} = c_{i,\sigma}^\dagger c_{i,\sigma}$ are number operators. The ratio U/t controls the degree of correlation in the system.

For the two-site Hubbard model at half filling in the site basis with spin projection $m_s = 0$, we consider first the convergence of the four projectors when the true ground state energy is known, with results shown in Fig. 3. We find that in this scenario, the performance of the wall-Chebyshev projector is similar to that of the eigenstate filtering algorithm, with both converging significantly faster than the step function based projector and the imaginary time evolution. For large U , the wall-Chebyshev projector converges up to six times faster than the eigenstate filtering approach. However, the difference in performance between the four approaches is particularly stark if the true ground-state energy is not known. The lowest energy single-determinant wavefunction in this system, corresponding to the $1^\alpha 2^\beta$ configuration or its spin-flipped pair, has zero energy at any U/t ratio. If we use this as an initial guess for the ground state energy S , the performance of the four projectors is shown in Fig. 4. For these results we used a value of $\alpha = 1.1$, although testing other values up to $\alpha = 1.5$ showed very similar performance. As an example, for $U=1$, in this mapping $R = 3.3$, the true ground state corresponds to $x \approx -1.946$ and the highest excited state to $x \approx 0.552$.

In this case, the wall-Chebyshev and imaginary time evolution projectors show similar convergence characteristics as before, while both the eigenstate filtering and the step function projector fail to converge to the correct state. We can understand this behaviour by considering the effect of the polynomials onto an arbitrary wavefunction in both scenarios, as seen in Fig. 5. In the case of

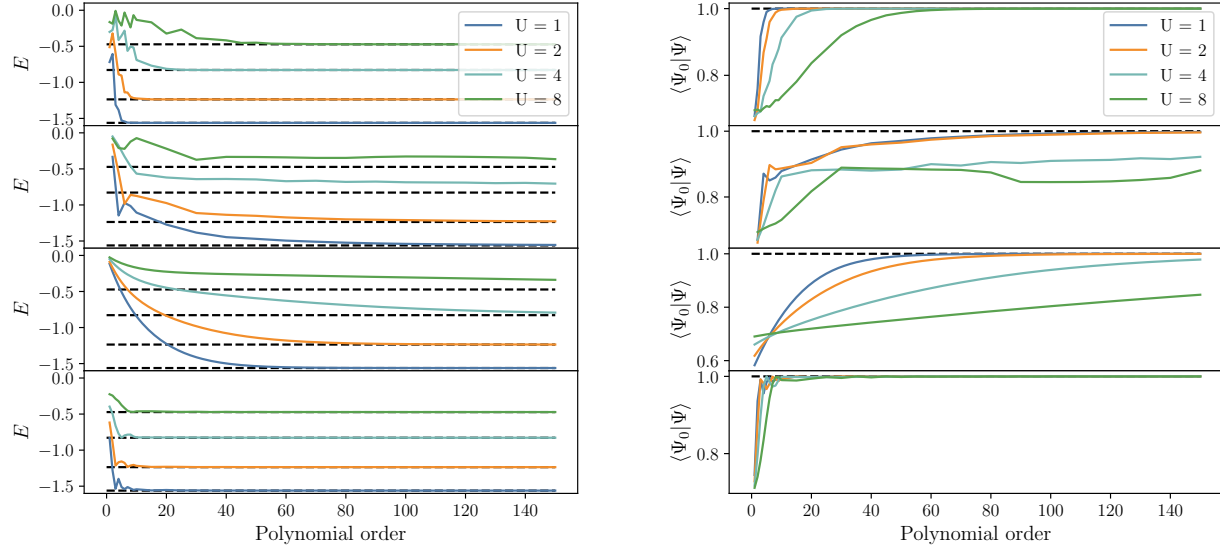


FIG. 3. Projector convergence onto the ground state of the two-site Hubbard model with $t = 1$ and different values of U . The projectors use, from the top, are the eigenstate filter, the step function projector, the imaginary time evolution projector and the wall-Chebyshev projector. The left panels show energy convergence, while the right show fidelity with the ground state wavefunction, as a function of polynomial order. In all cases, the ground state energy is known *a priori* and given as a parameter to the projector.

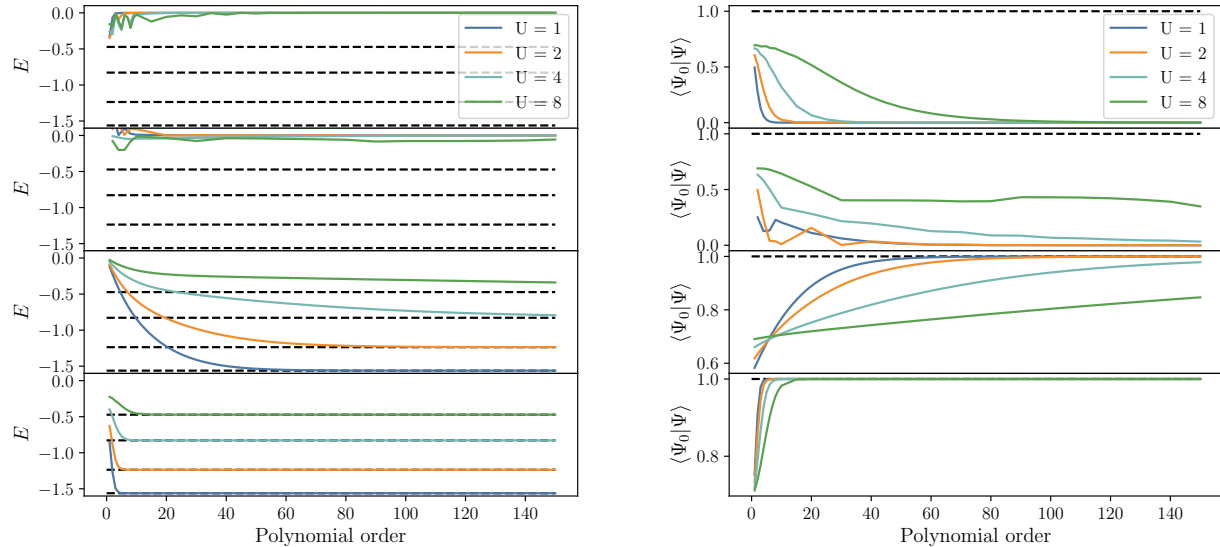


FIG. 4. Projector convergence onto the ground state of the two-site Hubbard model with $t = 1$ and different values of U . The projectors used are, from the top, the eigenstate filter, the step function projector, the imaginary time evolution projector and the wall-Chebyshev projector. The left panels show energy convergence, while the right show fidelity with the ground state wavefunction, as a function of polynomial order. In all cases, the ground state energy is estimated as the energy of the Hartree-Fock state.

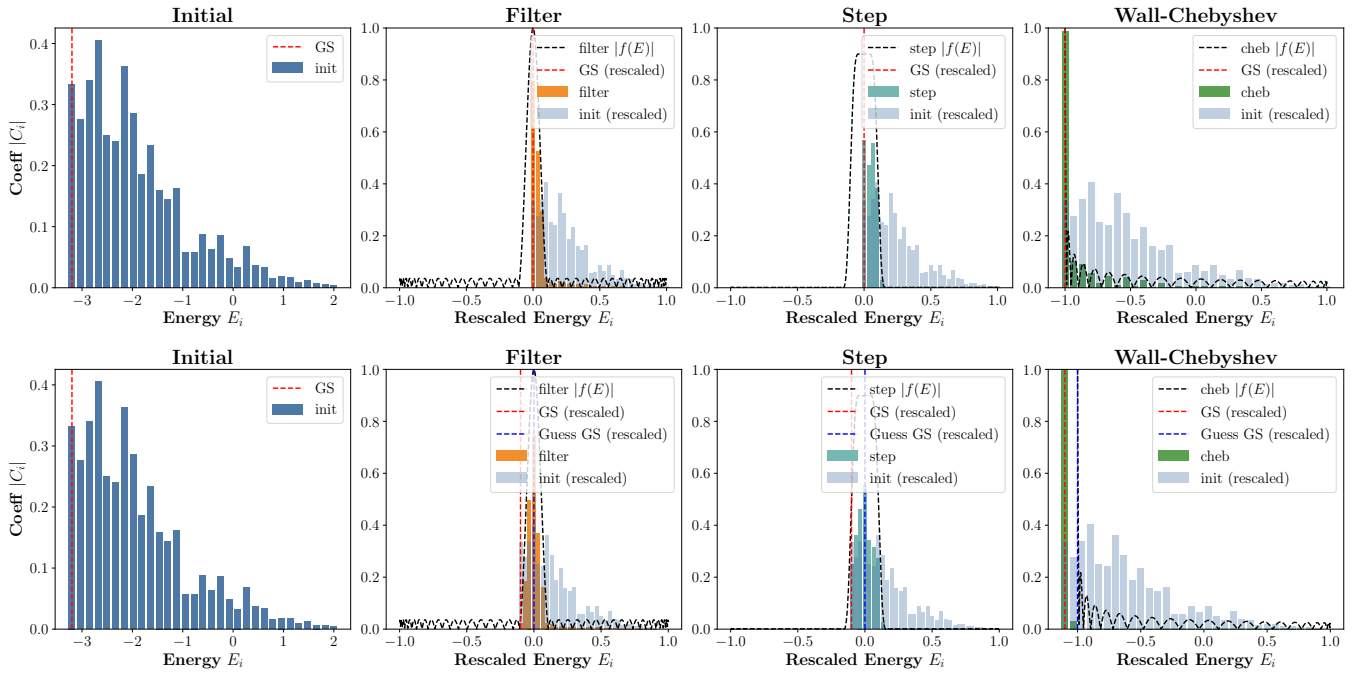


FIG. 5. Comparison of different projectors: eigenstate filter (orange), step function (turquoise) and wall-Chebyshev (green) ground state projectors of an arbitrary Hamiltonian H , given knowledge of the exact ground state (top) or an approximation (bottom). The filter and wall-Chebyshev polynomials are approximated by a degree 20 polynomial, while the step function is approximated by a 100 degree polynomial, necessary to capture the flat top of the function. Showing their respective action on an initial state (blue) $|\Psi\rangle = \sum_i C_i |\phi_i\rangle$, where each bar corresponds to $|\phi_i\rangle$ and is an eigenvector with an expansion coefficient C_i (shown on the y axis) and a corresponding eigenvalue E_i (shown on the x axis). The projection acts via a renormalisation of $|\Psi'\rangle = \sum_i f(E_i) C_i |\phi_i\rangle$. Where $|\Psi'\rangle$ is the projected state and $|f(E_i)|$ is the absolute value of the respective projection function on the eigenvalues at E_i (dotted black). For each projector, the rescaled initial state is shown for comparison (light blue). The lowest energy in each case is the ground state of H .

the eigenstate filter and step function, the guess for the ground state energy is used as the 0 of the rescaled Hamiltonian, while in the wall-Chebyshev case it corresponds to -1 . If the true ground state is below this value, in the eigenstate filter case it will fall outside the width of the δ function, causing the contribution of the ground state to be damped. In the step function case, the main issue is the existence of excited states between the ground state and the estimate, which will also be left unchanged by the step function, rather than being damped. In the wall-Chebyshev case, the ground state now falls outside the $[-1, 1]$ interval, where the function goes steeply towards infinity. As such, it will continue to be the most undamped contribution to the wavefunction even if the guess energy is not exact. While not shown in Fig. 5, the same argument applies to the conventional imaginary time evolution operator. We note that, due to the rescaling required to apply the Hamiltonian through the LCU, the wall-Chebyshev projector does not in practice over-express the ground state if it lies below -1 , as could be expected from Fig. 1, but rather more strongly damps other contributions in order to maintain normalisation of the resulting wavefunction. This leads to a faster convergence to the ground state, at the cost of lower success probability in applying the operator, as more information is lost upon application. As can be seen from Fig. 6, this is not a problem unless the initial overlap with the ground state is quite low.

The Hubbard model is pathological in this scenario, as (a) the single-determinant energy is much higher than the ground state and (b) there are eigenstates of the Hubbard Hamiltonian which are degenerate to this single-determinant, making it impossible for the step function to select a single eigenstate.

In Fig. 7, we consider the performance of the projectors with an increasing number of sites, using the fidelity to the ground state as the convergence metric. We only consider the step function for two- and four-site Hubbard models as the small spacing between the ground and first excited state in larger models made it difficult to converge. As the imaginary time evolution projector is guaranteed to be slower than the wall-Chebyshev, we do not report results for it here. We observe the same patterns as before, with faster convergence of the wall-Chebyshev projector relative to alternative methods as the number of sites increases. Both other algorithms fail when the HF energy is taken as an approximation of the ground state, and the step function projector additionally fails in the 4-site case even when an exact estimate of the energy is given.

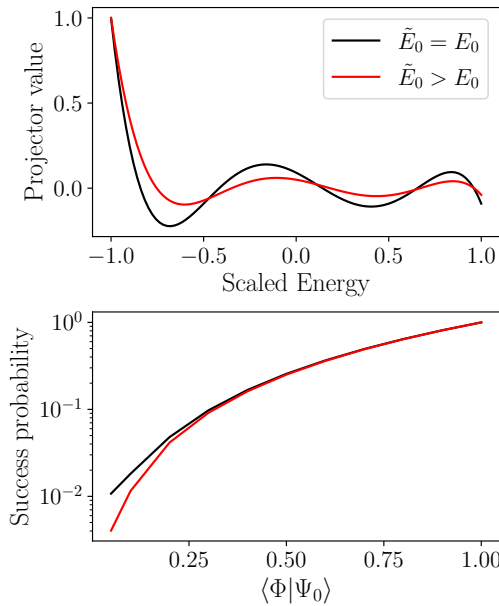


FIG. 6. Effect of overestimating the ground-state energy in a quantum wall-Chebyshev projector. **Top:** Value of the projector as a function of scaled energy eigenvalue. **Bottom:** Success probability of applying the projector as a function of initial overlap with the ground state, assuming maximum allowed subnormalisation α .

As noted above, the Hubbard model is particularly difficult for preexisting methods to get right in the absence of a very good energy estimate. We now consider a system less challenging from this perspective, in the form of hydrogen chains H_n with $2 \leq n \leq 6$ in the STO-3G basis set. In Table II, we present the order of each projector needed to obtain errors below 1 mHartree in the ground state energy for each system, restricting ourselves to the more quickly converging eigenstate filter and wall-Chebyshev projectors. At short bond lengths, where Hartree-Fock provides a good approximation for the ground state of the system, the eigenstate filter outperforms the wall-Chebyshev projector for H_2 even when the Hartree-Fock energy is used as an estimate for E_0 . However, as the bond length is stretched and the HF energy moves away from the ground state, the wall-Chebyshev operator becomes once again dominant, requiring a constant polynomial order for convergence at all geometries. Additionally, even if the ground-state energy is known, the eigenstate filter convergence deteriorates more sharply with increasing bond length, likely due to the explicit dependence on the gap between the ground and first excited states. For H_4 the difference in performance is much more significant, with the eigenstate filter failing to converge within a polynomial order of 150 for all but the most compressed geometry. For the wall-Chebyshev projector, a maximum order of 50 is sufficient for convergence in all systems.

VI. CONCLUSION

We present in this paper a novel ground state projector based on a Chebyshev expansion of the wall function. At finite order, the roots of this expansion have a known closed form, allowing the projector to be expressed as a product of linear Hamiltonian terms. As the roots are known *a priori*, each of these terms can be implemented independently, requiring no additional ancilla relative to the Hamiltonian oracle itself. Like in the case of fragmented imaginary time evolution, this approach allows successful application of each term to be verified, making it possible to abort unsuccessful attempts early. Decaying success probabilities remain problematic for ground state projectors, but this can be mitigated through amplitude amplification[41] techniques, as is customarily done in QSP-based projectors[32, 42].

Method	$r_{H-H}/\text{\AA}$	Known E_0			Unknown E_0		
		H_2	H_4	H_6	H_2	H_4	H_6
wall-Chebyshev	1.00	3	7	12	3	6	8
	1.50	5	11	22	3	7	11
	2.00	5	14	37	3	6	24
	2.50	15	18	46	3	6	12
	3.00	10	25	49	3	6	12
Eigenstate filter	1.00	2	51	-	2	53	-
	1.50	3	-	-	44	-	-
	2.00	31	-	-	23	-	-
	2.50	17	-	-	47	-	-
	3.00	55	-	-	27	-	-

TABLE II. Polynomial order at which the energy of the state obtained by applying a projector first has an error of less than 1 mHartree relative to the true ground state energy for H_n molecules in the STO-3G basis. A maximum polynomial order of 150 was used.

We show that the wall-Chebyshev projector leads to a polynomial improvement in asymptotic scaling compared to pre-existing approaches based on imaginary time-evolution or alternative function approximations. Numerically, it is shown to outperform projectors based on step functions and delta functions for strongly correlated model systems and a molecular example. Additionally, it preserves a desirable property of imaginary time evolution itself: the ground state amplitude is most weakly damped in the resulting state, regardless of whether a good estimate of the ground state energy is known. Having such an estimate remains desirable, as it generates better success probability of applying the projector.

ACKNOWLEDGEMENTS

We thank Yuta Kikuchi and Michelle Sze for their helpful comments on this work. MAF gratefully ac-

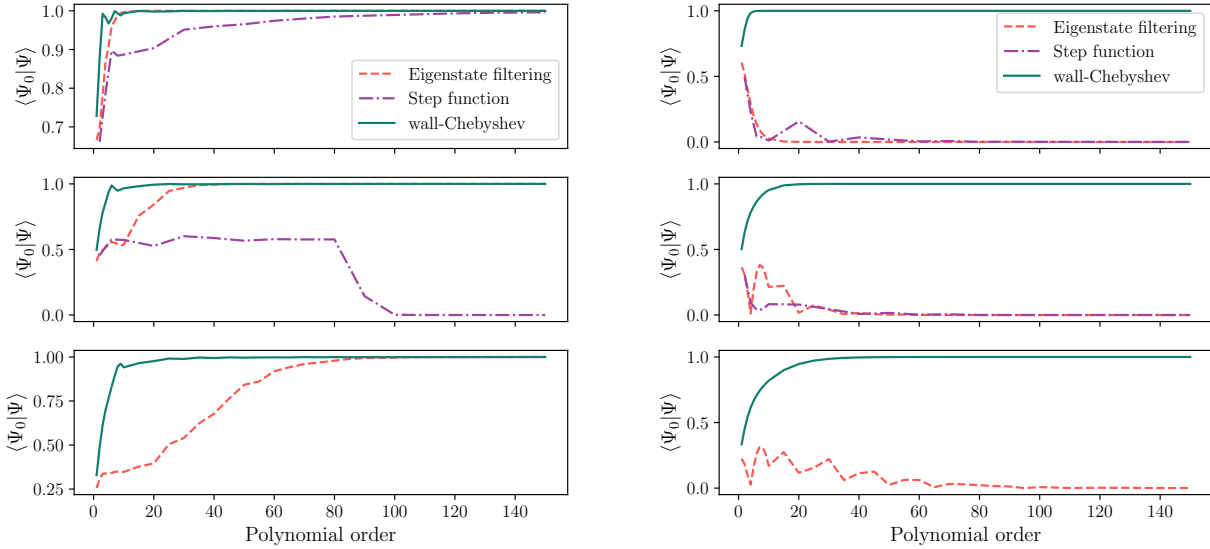


FIG. 7. Convergence onto the ground state of the half-filled Hubbard model with $t = 1$, $U = 2$, and two (top), four (middle) or six (bottom) sites, using different ground state projectors. The panels show fidelity with the ground state wavefunction, when the ground state energy is known *a priori* (left) or not (right).

knowledges Peterhouse, Cambridge for financial support

through a Research Fellowship.

[1] G. C. Wick, Properties of bethe-salpeter wave functions, *Phys. Rev.* **96**, 1124 (1954).

[2] H. G. A. Burton, Energy landscape of state-specific electronic structure theory, *J. Chem. Theory Comput.* **18**, 1512 (2022).

[3] Choy B., M.-A. Filip, and D. J. Wales, Energy landscapes for the unitary coupled cluster ansatz, *Journal of Chemical Theory and Computation* **21**, 1739 (2025).

[4] T. Jones, S. Endo, S. McArdle, X. Yuan, and S. C. Benjamin, Variational quantum algorithms for discovering hamiltonian spectra, *Phys. Rev. A* **99**, 062304 (2019).

[5] S. McArdle, T. Jones, S. Endo, S. C. B. Ying Li, and X. Yuan, Variational ansatz-based quantum simulation of imaginary time evolution, *npj Quantum Inf* **5**, 75 (2019).

[6] M. Benedetti, M. Fiorentini, and M. Lubasch, Hardware-efficient variational quantum algorithms for time evolution, *Phys. Rev. Res.* **3**, 033083 (2021).

[7] X. Yuan, S. Endo, Q. Zhao, Y. Li, and S. C. Benjamin, Theory of variational quantum simulation, *Quantum* **3**, 191 (2019).

[8] J. R. McClean, S. Boixo, V. N. Smelyanskiy, R. Babbush, and H. Neven, Barren plateaus in quantum neural network training landscapes, *Nat. Commun.* **9** (2018).

[9] M. Motta, C. Sun, A. T. K. Tan, M. J. O'Rourke, E. Ye, A. J. Minnich, F. G. S. L. Brandão, and G. K.-L. Chan, Determining eigenstates and thermal states on a quantum computer using quantum imaginary time evolution, *Nat. Phys.* **16** (2020).

[10] H. Nishi, T. Kosugi, and Y. Matsushita, Implementation of quantum imaginary-time evolution method on nisq devices by introducing nonlocal approximation, *npj Quantum Inf* **7** (2021).

[11] S.-N. Sun, M. Motta, R. N. Tazhigulov, A. T. Tan, G. K.-L. Chan, and A. J. Minnich, Quantum computation of finite-temperature static and dynamical properties of spin systems using quantum imaginary time evolution, *PRX Quantum* **2**, 010317 (2021).

[12] T. Liu, J. Liu, and H. Fan, Probabilistic nonunitary gate in imaginary time evolution, *Quantum Inf Process* **20** (2021).

[13] T. Kosugi, Y. Nishiya, H. Nishi, and Y.-i. Matsushita, Imaginary-time evolution using forward and backward real-time evolution with a single ancilla: First-quantized eigensolver algorithm for quantum chemistry, *Phys. Rev. Res.* **4**, 033121 (2022).

[14] F. Turro, A. Roggero, V. Amitrano, P. Luchi, K. A. Wendt, J. L. Dubois, S. Quaglioni, and F. Pederiva, Imaginary-time propagation on a quantum chip, *Phys. Rev. A* **105**, 022440 (2022).

[15] T. L. Silva, M. M. Taddei, S. Carrazza, and L. Aolita, Fragmented imaginary-time evolution for early-stage quantum signal processors, *Sci. Rep.* **13** (2023).

[16] C. Leadbeater, N. Fitzpatrick, D. Muñoz Ramo, and A. J. W. Thom, Non-unitary trotter circuits for imaginary time evolution, *Quantum Science and Technology* **9**, 045007 (2024).

[17] Y. Dong, L. Lin, and Y. Tong, Ground-state preparation and energy estimation on early fault-tolerant quantum computers via quantum eigenvalue transformation of unitary matrices, *PRX Quantum* **3**, 040305 (2022).

[18] H. H. S. Chan, D. M. Ramo, and N. Fitzpatrick, Simulating non-unitary dynamics using quantum signal processing with unitary block encoding (2023), [arXiv:2303.06161 \[quant-ph\]](https://arxiv.org/abs/2303.06161).

[19] J. B. Anderson, Quantum chemistry by random walk. H ^2P , $\text{H}_3^+ \text{D}_{3h} \text{A}'_1$, $\text{H}_2 \text{^3\Sigma}_u^+$, $\text{H}_4 \text{^1\Sigma}_g^+$, Be ^1S , *The Journal of Chemical Physics* **65**, 4121 (1976), https://pubs.aip.org/aip/jcp/article-pdf/65/10/4121/18904095/4121_1_online.pdf.

[20] S. Zhang and H. Krakauer, Quantum monte carlo method using phase-free random walks with slater determinants, *Phys. Rev. Lett.* **90**, 136401 (2003).

[21] G. H. Booth, A. J. W. Thom, and A. Alavi, Fermion Monte Carlo without fixed nodes: A game of life, death, and annihilation in Slater determinant space, *J. Chem. Phys.* **131**, 054106 (2009).

[22] A. J. W. Thom, Stochastic Coupled Cluster Theory, *Phys. Rev. Lett.* **105**, 263004 (2010).

[23] N. H. Stair and F. A. Evangelista, Simulating many-body systems with a projective quantum eigensolver, *PRX Quantum* **2**, 030301 (2021).

[24] L. Lin and Y. Tong, Near-optimal ground state preparation, *Quantum* **4**, 372 (2020).

[25] L. Lin and Y. Tong, Optimal polynomial based quantum eigenstate filtering with application to solving quantum linear systems, *Quantum* **4**, 361 (2020).

[26] T. Zhang and F. A. Evangelista, A Deterministic Projector Configuration Interaction Approach for the Ground State of Quantum Many-Body Systems, *J. Chem. Theory Comput.* **12**, 4326 (2016).

[27] Z. Zhao, M.-A. Filip, and A. J. W. Thom, Rapidly convergent coupled-cluster monte carlo using a chebyshev projector (2024), [arXiv:2402.16685 \[cond-mat.str-el\]](https://arxiv.org/abs/2402.16685).

[28] S. Geršgorin, Über die Abgrenzung der Eigenwerte einer Matrix, *Bulletin de l'Académie des Sciences de l'URSS. Classe des sciences mathématiques et na*, 749 (1931).

[29] A. M. Childs and N. Wiebe, Hamiltonian simulation using linear combinations of unitary operations, *Quantum Inf. Comput.* **12**, 901,924 (2012).

[30] A. Gilyén, Y. Su, G. H. Low, and N. Wiebe, Quantum singular value transformation and beyond: exponential improvements for quantum matrix arithmetics, in *Proceedings of the 51st Annual ACM SIGACT Symposium on Theory of Computing*, STOC 2019 (Association for Computing Machinery, New York, NY, USA, 2019) p. 193–204.

[31] J. M. Martyn, Z. M. Rossi, A. K. Tan, and I. L. Chuang, Grand unification of quantum algorithms, *PRX Quantum* **2**, 040203 (2021).

[32] J. M. Martyn, Y. Liu, Z. E. Chin, and I. L. Chuang, Efficient fully-coherent quantum signal processing algorithms for real-time dynamics simulation, *The Journal of Chemical Physics* **158**, 024106 (2023), https://pubs.aip.org/aip/jcp/article-pdf/doi/10.1063/5.0124385/16668116/024106_1_online.pdf.

[33] D. Motlagh and N. Wiebe, Generalized quantum signal processing, *PRX Quantum* **5**, 020368 (2024).

[34] N. Fitzpatrick and M.-A. Filip, Wallcheb: Wall chebyshev ground state projectors in guppy, https://github.com/NathanCQC/wall_chebyshev (2025).

[35] M. Koch, A. Lawrence, K. Singhal, S. Sivarajah, and R. Duncan, Guppy: Pythonic quantum-classical programming, in *Informal Proceedings of the Fourth International Workshop on Programming Languages for Quantum Computing (PLanQC '24)* (2024).

[36] M. W. Sze, Y. Tang, S. Dilkes, D. M. Ramo, R. Duncan, and N. Fitzpatrick, Hamiltonian dynamics simulation using linear combination of unitaries on an ion trap quantum computer (2025), [arXiv:2501.18515 \[quant-ph\]](https://arxiv.org/abs/2501.18515).

[37] Y. Dong, X. Meng, K. B. Whaley, and L. Lin, Efficient phase-factor evaluation in quantum signal processing, *Phys. Rev. A* **103**, 042419 (2021).

[38] J. Wang, Y. Dong, and L. Lin, On the energy landscape of symmetric quantum signal processing, *Quantum* **6**, 850 (2022).

[39] Y. Dong, L. Lin, H. Ni, and J. Wang, Robust iterative method for symmetric quantum signal processing in all parameter regimes, *SIAM Journal on Scientific Computing* **46**, A2951 (2024), <https://doi.org/10.1137/23M1598192>.

[40] Y. Dong, L. Lin, H. Ni, and J. Wang, Infinite quantum signal processing, *Quantum* **8**, 1558 (2024).

[41] G. Brassard, P. Hoyer, M. Mosca, and A. Tapp, Quantum amplitude amplification and estimation, in *Quantum computation and information*, Contemporary Mathematics, Vol. 305 (2002) pp. 53–74.

[42] A. Gilyén, Y. Su, G. H. Low, and N. Wiebe, Quantum singular value transformation and beyond: exponential improvements for quantum matrix arithmetics, in *Proceedings of the 51st Annual ACM SIGACT Symposium on Theory of Computing*, STOC 2019 (Association for Computing Machinery, New York, NY, USA, 2019) p. 193–204.

[43] D. Elliott, D. Paget, G. Phillips, and P. Taylor, Error of truncated chebyshev series and other near minimax polynomial approximations, *Journal of Approximation Theory* **50**, 49 (1987).

Appendix A: Gershgorin circle theorem

The Gershgorin circle theorem[28] states that, for a complex matrix A with elements a_{ij} , one may define the closed Gershgorin discs $D(a_{ii}, R_i) \subseteq \mathbb{C}$, which are centred at a_{ii} and have radii

$$R_i = \sum_{j \neq i} |a_{ij}|. \quad (\text{A1})$$

Then, every eigenvalue λ_i of A must lie in at least one of the Gershgorin disks.

Since the Hamiltonian is a Hermitian matrix, both its eigenvalues and diagonal elements in any basis are always real. The Gershgorin theorem therefore reduces to

$$\min_i(a_{ii} - R_i) \leq \min_i \lambda_i \leq \max_i \lambda_i \leq \max_i(a_{ii} + R_i) \quad (\text{A2})$$

and provides both lower and upper bounds for the Hamiltonian eigenvalues. However, computing these bounds exactly is exponentially expensive and therefore impractical. Instead, we assume that $\max_i(a_{ii} + R_i) = a_{N-1,N-1} + R_{N-1}$ is the extreme of the Gershgorin disk corresponding to the highest excited determinant in the Hilbert space and use this as an estimate of the highest Hamiltonian eigenvalue. This is a likely, but not guaranteed scenario; however, this approximation has been found to work well in classical QMC[27], in particular when combined with a modest stretching factor that mitigates some of the risk of having underestimated the maximal eigenvalue.

Appendix B: Linear Combination of Unitaries

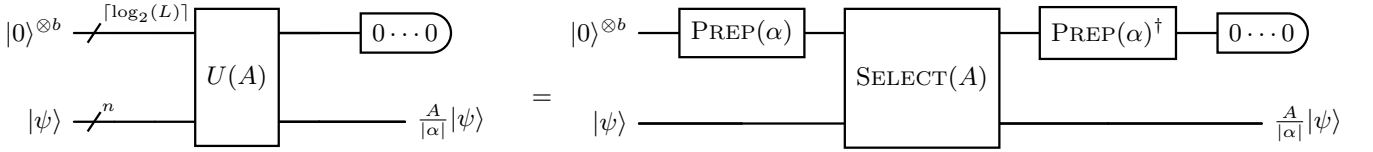


FIG. 8. LCU Circuit acting on an arbitrary quantum state $|\psi\rangle$ with a rescaled operator $\frac{A}{|\alpha|}$, when a successful post-selection occurs.

Consider an operator A , which may be written as

$$\hat{A} = \sum_{\ell=0}^L \alpha_{\ell} A_{\ell}, \quad (\text{B1})$$

where the operators A_{ℓ} are unitary. An $(\alpha, b, 0)$ block-encoding of A can then be implemented using the circuit given in Fig. 8, where $\alpha = \sum_{\ell=0}^L |\alpha_{\ell}|$ is the 1-norm of the operator A and $b = \lceil \log_2(L) \rceil$.

The LCU block-encoding is made up of two oracles, PREPARE and SELECT. The PREPARE oracle is a unitary matrix that transforms the all-zero state of the control register to a positive real state $|L\rangle$ that encodes the rescaled coefficient of the LCU. The full unitary matrix of the PREPARE oracle is given by:

$$\text{PREPARE} = \sum_{\ell=0}^{L-1} \sqrt{\frac{\alpha_{\ell}}{|\alpha|}} |\ell\rangle\langle 0| + \Pi_{\perp} = \begin{bmatrix} \sqrt{\frac{\alpha_0}{|\alpha|}} & \cdot & \dots \\ \sqrt{\frac{\alpha_1}{|\alpha|}} & \cdot & \dots \\ \vdots & \ddots & \dots \\ \sqrt{\frac{\alpha_{L-1}}{|\alpha|}} & \cdot & \dots \end{bmatrix}. \quad (\text{B2})$$

It can be seen that we only need to be concerned with the first column of the matrix if acting on the all-zero state. The SELECT oracle is a unitary matrix that acts on the state register and the PREPARE register. It indexes the unitaries in the LCU onto a control register $|\ell\rangle$ and applies the operator terms to the state register via a multi controlled operation for each term indexed by a unique prepare register bit string:

$$\text{SELECT}(H) := \sum_{\ell=0}^{L-1} |\ell\rangle\langle \ell| \otimes H_{\ell}. \quad (\text{B3})$$

The corresponding circuit is given in Fig. 9.

The standard LCU procedure involves initialising the PREPARE register in the state $|L\rangle = \sum_{\ell=0}^{L-1} \sqrt{\frac{\alpha_{\ell}}{|\alpha|}} |\ell\rangle$. Subsequently, the SELECT oracle is used to apply the operator terms onto the state register. After this operation, the prepare register is uncomputed, and the state register is measured in the computational basis.

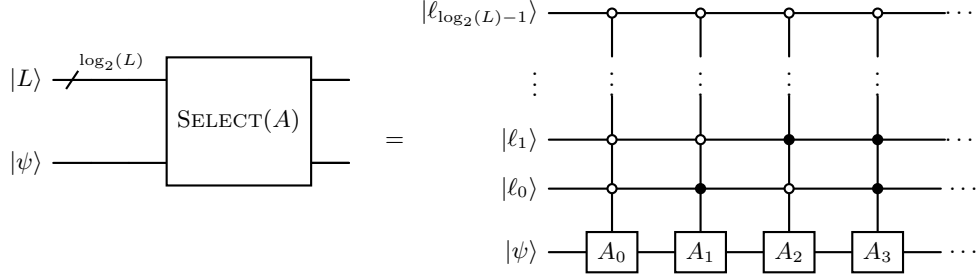


FIG. 9. SELECT circuit.

Appendix C: Quantum Singular Value Decomposition

The standard approach to encoding projectors for use in quantum computing is by quantum singular value transformation (QSVT)[30, 31]. For a given matrix A , with singular value decomposition

$$A = \sum_i \lambda_i |\tilde{\psi}_i\rangle \langle \tilde{\psi}_i|, \quad (C1)$$

we can define a singular value transformation as

$$f(A) = \begin{cases} \sum_i f(\lambda_i) |\tilde{\psi}_i\rangle \langle \tilde{\psi}_i|, & f \text{ odd} \\ \sum_i f(\lambda_i) |\psi_i\rangle \langle \psi_i|. & f \text{ even} \end{cases} \quad (C2)$$

Consider a block-encoding U of A , such that

$$A = \tilde{\Pi} U \Pi, \quad (C3)$$

where $\tilde{\Pi} = \sum_i |\tilde{\psi}_i\rangle \langle \tilde{\psi}_i|$ and $\Pi = \sum_i |\psi_i\rangle \langle \psi_i|$. The QSVT algorithm uses Quantum Signal Processing (QSP) to encode a polynomial function of $P(A)$ using a phased alternating sequence

$$U_\Phi \equiv \begin{cases} e^{i\phi_1 \tilde{\Pi}} U \prod_{k=1}^{(d-1)/2} \left(e^{i\phi_{2k} \Pi} U^\dagger e^{i\phi_{2k+1} \tilde{\Pi}} U \right), & d \text{ odd} \\ \prod_{k=1}^{d/2} \left(e^{i\phi_{2k-1} \Pi} U^\dagger e^{i\phi_{2k} \tilde{\Pi}} U \right), & d \text{ even} \end{cases} \quad (C4)$$

where $\Phi = \{\phi_0, \phi_1, \dots, \phi_d\} \in \mathbb{R}^{d+1}$ are the phases which encode the polynomial transform. If U is an $(\alpha, b, 0)$ -block encoding of A , U_Φ represents a $(1, b, 0)$ -block encoding of $P^{(SV)}(A/\alpha)$:

$$P^{(SV)} \left(\frac{A}{\alpha} \right) = \tilde{\Pi} U_\Phi \Pi. \quad (C5)$$

The corresponding phases can be calculated by classical optimisation. For the singular value decomposition to be well-defined, the polynomial P must obey the parity constraint detailed in the main text.

Appendix D: Wall-Chebyshev convergence factor

The convergence factor of a ground state projector is defined as $\gamma = -g'(E_0)$. For the wall-Chebyshev polynomial, we can rewrite Eq. (14) for numerical values of the the energy E as

$$x = 2 \frac{E - E_0}{R} - 1. \quad (D1)$$

Therefore,

$$\frac{dg_m^{\text{wall-Ch}}(E)}{dE} \bigg|_{E=E_0} = \frac{2}{R} \frac{dG_m^{\text{wall-Ch}}(x)}{dx} \bigg|_{x=-1}, \quad (D2)$$

with $G_m^{\text{wall-Ch}}$ and $g_m^{\text{wall-Ch}}$ defined according to Eqs. (13) and (15), respectively. The derivatives of Chebyshev polynomials are given by

$$\frac{dT_0(x)}{dx} = 0, \quad (\text{D3})$$

$$\frac{dT_1(x)}{dx} = 1, \quad (\text{D4})$$

$$\frac{dT_{2k}(x)}{dx} = (2k) \cdot 2 \sum_{j=1}^k T_{2j-1}(x), \quad \forall k \in \mathbb{N}_+, \quad (\text{D5})$$

$$\frac{dT_{2k+1}(x)}{dx} = (2k+1) \left[T_0(x) + 2 \sum_{j=1}^k T_{2j}(x) \right], \quad \forall k \in \mathbb{N}_+. \quad (\text{D6})$$

The derivative of the wall function projector is given by

$$\frac{dG_m^{\text{wall-Ch}}(x)}{dx} \Big|_{x=-1} = \frac{1}{2m+1} \left[\sum_{k=0}^m (2 - \delta_{k0}) (-1)^k \frac{dT_k(x)}{dx} \Big|_{x=-1} \right]. \quad (\text{D7})$$

Substituting Eqs. (D3) to (D6) and considering the case where $m = 2n + 1$ for simplicity, we find that

$$\begin{aligned} \frac{dG_m^{\text{wall-Ch}}(x)}{dx} \Big|_{x=-1} &= \frac{1}{2m+1} \left\{ \sum_{k=1}^n \left[2(-1)^{(2k)} (2k) \cdot 2 \sum_{j=1}^k T_{2j-1}(-1) \right] \right. \\ &\quad \left. + \sum_{k=1}^n \left[2(-1)^{(2k+1)} (2k+1) \left(T_0(-1) + 2 \sum_{j=1}^k T_{2j}(-1) \right) \right] - 2 \right\} \\ &= \frac{1}{2m+1} \left\{ \sum_{k=1}^n \left[2(-1)^{(2k)} (2k)(-2k) \right] \right. \\ &\quad \left. + \sum_{k=1}^n \left[2(-1)^{(2k+1)} (2k+1)(2k+1) \right] - 2 \right\} \\ &= -\frac{2}{2m+1} \left[2 + \sum_{k=1}^n (2k)^2 + \sum_{k=1}^n (2k+1)^2 \right] \\ &= -\frac{2}{2m+1} \sum_{k=0}^m k^2 \\ &= -\frac{2}{2m+1} \frac{m(m+1)(2m+1)}{6} \\ &= -\frac{m(m+1)}{3}. \end{aligned} \quad (\text{D8})$$

The convergence factor is therefore

$$\gamma = -\frac{2}{R} \left[-\frac{m(m+1)}{3} \right] = \frac{2m(m+1)}{3R}. \quad (\text{D9})$$

An equivalent calculation may be carried out for even m , leading to the same value of γ .

Appendix E: Complexity Analysis of Other Projectors

1. Imaginary time evolution

We follow the procedure of Ref. [15] to derive the scaling of a QSP approximation to the imaginary time evolution operator, for Hamiltonians with $\|H\| \leq 1$. Given a Hamiltonian with $\|H\| > 1$, it is possible to rescale it to [15]

$$H' = \frac{H - \bar{\lambda}I}{\Delta\lambda}, \quad (\text{E1})$$

where $\bar{\lambda} = (\lambda^+ + \lambda^-)/2$, $\Delta\lambda = \lambda^+ - \lambda^-$ and $\lambda^+(\lambda^-)$ is an upper (lower) bound to the largest (smallest) eigenvalue of H . The transformation $e^{-\tau H}$ can be recovered by $e^{-\tau' H'}$ where $\tau' = \Delta\lambda\tau$.

The imaginary time evolution operator can be expressed in terms of Chebyshev polynomials via the Jacobi–Anger expansion, as

$$f(H) = e^{-\tau H} = I_0(\tau) + 2 \sum_{k=1}^{\infty} (-1)^k I_k(\tau) T_k(H), \quad (\text{E2})$$

where I_k are the modified Bessel functions of the first kind. The error ϵ_{tr} of approximately synthesising $f(\hat{H})$ through a Chebyshev expansion $\tilde{f}_q(H) = \sum_{k=0}^q b_k T_k(H)$ is given by[15, 43]

$$\epsilon = \max_{-1 \leq \lambda \leq 1} |f(\lambda) - \tilde{f}(\lambda)| = \frac{|f^{(q+1)}(\xi)|}{2^q (q+1)!} \quad (\text{E3})$$

for some $\xi \in (-1, 1)$. Therefore,

$$\epsilon_{tr} \leq \frac{\max_{\lambda \in [\lambda_{\min}, \lambda_{\max}]} |f^{(q+1)}(\lambda)|}{2^{\frac{q}{2}} (q+1)!} \quad (\text{E4})$$

where $f^{(q+1)}$ is the $(q+1)$ -th derivative of f . Given

$$|f^{(q+1)}(\lambda)| = \tau^{(q+1)} e^{-\tau\lambda} \leq \tau^{(q+1)}, \quad (\text{E5})$$

$$\epsilon_{tr} \leq \frac{\tau^{q+1}}{2^q (q+1)!} \leq \sqrt{\frac{2}{\pi(q+1)}} \left(\frac{e\tau}{2(q+1)} \right)^{q+1} \leq \left(\frac{\tau e}{2q} \right)^q, \quad (\text{E6})$$

where we have used Stirlings approximation to the factorial and assumed $e\tau/2 \leq q$. Solving this equation for q leads to the query complexity of the QSP encoding of a polynomial of order q approximation of the imaginary time evolution operator.

For $t \in \mathbb{R}$ and $\varepsilon \in (0, 1)$, let us define the number $r(t, \varepsilon) \geq t$ as the solution to the equation

$$\varepsilon = \left(\frac{t}{r} \right)^r : r \in (t, \infty). \quad (\text{E7})$$

It can be shown that[42]

$$\begin{aligned} \forall t \geq \frac{\ln(1/\varepsilon)}{e}, \quad r(t, \varepsilon) &\leq et, \\ \forall t \leq \frac{\ln(1/\varepsilon)}{e}, \quad r(t, \varepsilon) &\leq \frac{4 \ln(1/\varepsilon)}{\ln(e + \ln(1/\varepsilon)t)} \end{aligned} \quad (\text{E8})$$

and therefore

$$r(t, \varepsilon) = \mathcal{O} \left(t + \frac{\ln(1/\varepsilon)}{\ln(e + \ln(1/\varepsilon)t)} \right). \quad (\text{E9})$$

In this particular case, $t = \tau e/2$ and therefore

$$q(\tau, \epsilon_{tr}) = \mathcal{O} \left(\frac{e\tau}{2} + \frac{\ln(1/\epsilon_{tr})}{\ln(e + 2 \ln(1/\epsilon_{tr})/(e\tau))} \right). \quad (\text{E10})$$

If the aim of ITE is to obtain the ground state of the system, then the propagation time τ depends on the desired fidelity $f(\tau)$. By the same reasoning as before,

$$\begin{aligned}\epsilon(\tau) &= 1 - f(\tau) \\ &= 1 - \frac{1}{\sqrt{1 + \sum_{i>0} \left(\frac{c_i}{c_0}\right)^2 e^{-2\tau(E_i - E_0)}}} \\ &\leq \frac{1}{c_0} \frac{\sqrt{\sum_{i>0} c_i^2 e^{-2\tau(E_i - E_0)}}}{1 + \sqrt{\sum_{i>0} \left(\frac{c_i}{c_0}\right)^2 e^{-2\tau(E_i - E_0)}}}.\end{aligned}\tag{E11}$$

Therefore,

$$\tau = \mathcal{O}(\Delta^{-1} \log(\epsilon^{-1} c_0^{-1})).\tag{E12}$$

Assuming this corresponds to the regime where $\tau e/2 > \log(1/\epsilon_{\text{tr}})/e$, this implies that

$$q(\epsilon) = \mathcal{O}(\Delta^{-1} \log(\epsilon^{-1} c_0^{-1})).\tag{E13}$$

2. Eigenstate filtering

The eigenstate filtering algorithm of Lin and Tong[25] uses the polynomial of order $2l$ given in Eq. (9) to approximate the projector onto the eigenstate with eigenvalue λ :

$$P_\lambda \approx R_l(\tilde{H}; \tilde{\Delta}_\lambda),\tag{E14}$$

where $\tilde{H} = (H - \lambda I)/(\alpha + |\lambda|)$ and $\tilde{\Delta}_\lambda$ is the separation of the λ eigenvalue from the rest of the spectrum of \tilde{H} . The R_l polynomial has the property (Ref. 25, Lemma 2) that

$$\begin{aligned}|R_l(x; \Delta)| &\leq 2e^{-\sqrt{2}l\Delta}, \quad \forall 0 < \Delta \leq \frac{1}{12} \text{ and} \\ &\forall x \in [-1, -\Delta] \cap [\Delta, 1].\end{aligned}\tag{E15}$$

This in turn guarantees that

$$|R_l(\tilde{H}, \tilde{\Delta}_\lambda) - P_\lambda| \leq 2e^{-\sqrt{2}l\tilde{\Delta}},\tag{E16}$$

so in order to obtain the ground state with fidelity higher than $1 - \epsilon$ one requires a number of queries to the Hamiltonian oracle that scales as

$$q(\epsilon) \propto l = \mathcal{O}(\Delta^{-1} \log(\epsilon^{-1} c_0^{-1})).\tag{E17}$$

This is the same asymptotic scaling as the ITE projector.

3. Step function projector

The construction of the step function projector in [24] is based on constructing a block encoding of the reflection operator,

$$R_{<\mu} = \sum_{k: \lambda_k < \mu} |\Psi_k\rangle \langle \Psi_k| - \sum_{k: \lambda_k > \mu} |\Psi_k\rangle \langle \Psi_k|.\tag{E18}$$

Given an $(\alpha, m, 0)$ -block-encoding of the Hamiltonian H , one can easily construct an $((\alpha + |\mu|, m + 1, 0)$ -block-encoding of $H - \mu I$ and then, using QSP, an $(1, m + 2, 0)$ -block encoding of the polynomial $-S(\frac{H - \mu I}{\alpha + |\mu|}; \delta, \epsilon)$. This is a polynomial of order $l = \mathcal{O}(\delta^{-1} \log(\epsilon^{-1}))$, which is defined such that

$$\forall x \in [-1, 1], \quad |S(x; \delta, \epsilon)| \leq 1,\tag{E19}$$

$$\forall x \in [-1, -\delta] \cup [\delta, 1], \quad |S(x; \delta, \epsilon) - \text{sgn}(x)| \leq \epsilon.\tag{E20}$$

When the separation between μ and any eigenvalue is at least $\Delta/2$ and $\delta = \Delta/4\alpha$, this corresponds to a $(1, m+2, \epsilon)$ -block-encoding of $R_{<\mu}$.

An $(1, m+3, \epsilon/2)$ encoding of the projector

$$P_{<\mu} = \sum_{k; \lambda_k < \mu} |\Psi_k\rangle \langle \Psi_k| = \frac{1}{2}(R_{<\mu} + I) \quad (\text{E21})$$

can then be block-encoded using the encoding of $R_{<\mu}$ and an additional ancilla. Given the scaling of the polynomial S and the definition of δ , each of these encodings requires $\mathcal{O}(\frac{\alpha}{\Delta} \log(\epsilon^{-1}))$ calls to the block encoding of the Hamiltonian. Given an initial wavefunction with overlap $\langle \Psi_0 | \Phi \rangle \geq c_0$ with the ground state, for final fidelity $1 - \epsilon$, an error less than $c_0\epsilon/2$ is needed in the projector.

$$\frac{\langle \Psi_0 | \tilde{P}_{<\mu} | \Phi \rangle}{\| \tilde{P}_{<\mu} | \Phi \rangle \|} \geq \frac{|\langle \Psi_0 | \Phi \rangle| - c_0\epsilon/2}{|\langle \Psi_0 | \Phi \rangle| + c_0\epsilon/2} \geq 1 - \frac{c_0\epsilon}{|\langle \Psi_0 | \Phi \rangle|} \geq 1 - \epsilon. \quad (\text{E22})$$

Therefore, the number of calls to the Hamiltonian oracle overall scales as $\mathcal{O}(\Delta^{-1} \log(c_0^{-1} \epsilon^{-1}))$. If amplitude amplification is used to increase the success probability to unity, the scaling increases to $\mathcal{O}(\Delta^{-1} c_0^{-1} \log(c_0^{-1} \epsilon^{-1}))$.